Using Mass-Spin Correlations to Probe the Tidal Spin-up and Formation Origins of Binary Black Holes

September 23, 2023

Author: April Qiu Cheng (aqc@mit.edu)
Direct Supervisor: Jacob Golomb (jgolomb@caltech.edu)
Faculty Supervisor: Alan Weinstein (ajw@caltech.edu)

Abstract

Gravitational waves contain information about the properties of the binary black holes (BBHs) that produce them, such as their masses and spins. With 69 confident (FAR $< 1\,\mathrm{yr}^{-1}$) BBHs in the third Gravitational Wave Transient Catalog (GWTC-3), it becomes possible to deduce bulk population properties of merging black holes (BHs) and hence probe their formation origins. Recent theoretical work has suggested that it is possible for the second-evolved BH to attain non-zero spin via tidal forces, and that this spin should be correlated with its mass. We construct a simple heuristic model that correlates the mass and spin of the higher-spinning BH. We evaluate its validity as a probe of the field formation scenario by hierarchically analyzing mock BBH detections drawn from an astrophysical distribution. We show that the model mis-specification from assuming a simple linear correlation can lead to the misleading conclusion that the underlying distribution broadens as we move farther away from the pivot mass. Finally, we also fit these models to GWTC-3 data.

1 Introduction

Gravitational waves (GWs)—first prediced by Einstein shortly after his introduction of General Relativity but at the time predicted to be unobservable—are propagating perturbations in the spacetime metric. In 2015, they were directly detected by the Laser Interferometer Gravitational-wave Observatory (LIGO) [1]. Since gravitational waves are produced by a time-varying mass quadrupole moment, thus far only merging binary compact objects (BHs and neutron stars) have produced gravitational waves detectable by our current gravitational wave experiments LIGO and Virgo [3]. Nonetheless, this has opened up an entirely new field of GW astronomy. With the third LIGO-Virgo GW Transient Catalog (GWTC-3), we have now $\mathcal{O}(100)$ detections of gravitational waves, most of which are BBHs. It is now possible to not only infer individual source properties, but also to probe the underlying population from which these BBHs arise, placing constraints on models of stellar evolution and astrophysics. Interesting population properties that can be probed with the GW dataset include the shape of the BH mass distribution [28, 2], the BH spin distribution [27, 8, 14, 34, 2], the distribution of BBHs across the sky [23], the evolution of merger rate and other properties with redshift [13, 8, 2], correlations between properties such as mass and spin [8, 15, 35, 5, 2, 19], and even branching ratios between different BBH formation channels [36, 18, 33, 24].

Such analyses are usually done with a method called hierarchical Bayesian inference. BBH systems are completely described by 15 parameters: two characterizing the mass of each BH, six characterizing the 3D spin vectors of each BH, and seven extrinsic parameters that describe the sky location, distance, and orientation of the system. However, these parameters cannot be extracted straightforwardly from the GW strain data; for example, the majority of the spin information we obtain from a detection is from a measurement of the effective dimensionless spin parameter ($\chi_{\rm eff}$), which is a mass-weighted combination of the spin magnitude projected onto the orbital angular momentum, since it is included in the leading-order term in the post-Newtonian expansion of the GW strain from a BBH merger. Furthermore, there exist degeneracies between some of the parameters. In the GW literature, these parameters are extracted using the strain data from each system using Bayesian inference in a process called parameter estimation (PE). Therefore, what we have for each detection is not an exact measurement of any parameter, but rather a 15-dimensional *posterior distribution* describing the probability that the system has a certain set of parameters, given the detected signal. It is these posterior distributions that are then used to infer properties of the underlying population. One can then choose an astrophysically-motivated parameterization of the population and fit the posterior samples to the model in another layer of Bayesian inference in a process called hierarchical Bayesian analysis, the output of which is a posterior distribution on the value of the population parameters; it is also possible to compare the likelihoods between the models to discern which one is more favored by the data. Analyses using flexible approaches (e.g. splines, Gaussian processes), which have the advantage of not being less model-dependent, have also been explored. See [32] for a pedagogical introduction to both PE and hierarchical inference in the context of GW astronomy.

One of the primary goals of hierarchical inference in GW astronomy is to learn about the formation origins of the detected BBHs. Several different formation mechanisms have been explored in the literature, each of which have different signatures in BBH parameter space, subject to modelling uncertainties. These formation channels can be roughly grouped into two categories: dynamical formation channels, which involve BBHs formed via random dynamical capture in dense stellar environments, and field channels, which involve the isolated co-evolution of a binary star system. Recent literature has suggested that while BHs born in isolation have close to zero spin due to efficient angular momentum transport out of the system during the core-collapse supernova [17], BBHs formed via field channels have the potential to be spun up via tidal excitations of oscillation modes in the secondary star by the BH companion [6]. This tidal spin-up is more efficient in lower mass systems, leading to a negative correlation between the mass and the spin magnitude of the spun-up secondary. Hierarchical mergers in dynamical channels, involving the mergers of merger remnants, also have a mass-spin correlation, as the 2nd-generation component should have both a higher mass and a characteristic high spin magnitude of around $a \sim 0.7$ [18]. Additionally, there are detections in our current catalog with extreme mass-spin properties that are difficult to explain via isolated evolution [35].

In this project, we probe mass-spin correlations in GW observations of BBHs with simple, heuristic linear models, similar to the models of [10, 8]. The goal of this project is to investigate the effectiveness and inherent biases of such a model to recover the correlations of the more complex astrophysical correlations given in [6], as well as the effect of contamination by hierarchical mergers of dynamically formed BBHs on this analysis. To do so, we draw simulated BBHs from an astrophysical distribution and inject them into the noise of various future detectors to create a mock catalog which we then analyze with hierarchical Bayesian inference. Finally, we also perform this inference on GWTC-3 data.

The structure of this paper will be as follows. In Section 2, we describe the models that we use. In Section 3, we describe our implementation of hierarchical Bayesian inference and our method

for drawing injected BBHs. We present our results in Section 4 and conclude in Section 6.

2 Models

In the standard literature, labels for each BH are assigned based on mass-sorting, i.e. m_1 and a_1 are the mass and spin of the BH with greater mass, while m_2 and a_2 correspond to the secondary BH. In our models, we employ the spin-sorting method pioneered by [7], such that m_A and a_A refer to the higher-*spinning* BH while m_B and a_B refer to the lower-spinning BH, such that $a_A > a_B$. We use this approach because we would like to target the correlation between the mass and spin of the star that is spun-up. While models suggest that this should be the secondary BH, it is possible that the second mass-transfer phase can result in mass ratio reversals. Additionally, many BBH systems have mass ratios close to unity, which makes it difficult to discern which is truly the secondary star. Furthermore, this approach is more agnostic towards the mechanism behind the mass-spin correlation and simply targets a correlation between the mass and spin of the higher-spinning star.

In all of our models, we use the source-frame masses. We use the `Power Law + Peak` model [28] to model the masses and a power law model [13] for the redshift; there are 9 hyperparameters across both models. We simultaneously fit both models with a spin distribution. Due to the limited data quality and number of current detections, we only allow for a linear dependence of the spin on the masses. Assuming that the majority of the detected BBHs originate from the field, this should capture, to first order, the correlation described in the previous section. In the following subsections, we lay out the different spin models which we employ, all of which model spin parameters as truncated Gaussians with log standard deviations and means allowed to vary linearly as a function of mass, as in [10, 8].

2.1 a_A spin model

The first model, which we call `a_A`, is astrophysically motivated and specifically targets the correlation between the mass and spin of the spun-up star described in [21]. We model a_A as a Gaussian truncated on $[0, 1]$ that is allowed to vary linearly with m_A, and model a_B as a Gaussian truncated on $[0, a_A]$ (hence enforcing the condition $a_A > a_B$) with a mean fixed at 0 and standard deviation that we fit for:

$$\pi(a_A \,|\, \Lambda, m_A) = \mathcal{N}(a_A;\, \mu_A(m_A, \Lambda), 10^{\log \sigma_A(m_A, \Lambda)}, 0, 1) \tag{1}$$

$$\pi(a_B \,|\, \Lambda, a_A) = \mathcal{N}(a_B;\, 0, \sigma_B, 0, a_A) \tag{2}$$

where $\mathcal{N}(x;\, \mu, \sigma, c, d)$ is a Gaussian on x truncated on $[c, d]$ with mean μ and standard deviation σ, $\Lambda = [\mu_{A0}, \delta_{\mu,\, AA}, \log \sigma_{A0}, \delta_{\log \sigma,\, AA}, \sigma_B]$ are the 5 spin hyperparameters, and

$$\mu_A(m_A, \Lambda) = \mu_{A0} + \delta_{\mu,\, AA} \left(\frac{m_A}{10\, M_\odot} - 1 \right) \tag{3}$$

$$\log \sigma_A(m_A, \Lambda) = \log \sigma_{\mathrm{A0}} + \delta_{\log \sigma,\, AA} \left(\frac{m_A}{10\, M_\odot} - 1 \right). \tag{4}$$

The a_B model models the star which is not tidally spun up; it is motivated by the finding that BHs born in isolation have close to zero spin [17] due to efficient angular momentum transport. We fit for σ_B to allow for spin from sources such as supernova kicks or angular momentum transport

that is not perfectly efficient. We additioally enforce the following conditions on the truncated Gaussian:

$$\mathcal{N}(x;\,\mu,\sigma,c,d) = \begin{cases} 0 & \text{if } \sigma < 10^{-3} \text{ or } \mu \notin [c-3\sigma, d+3\sigma] \\ \mathcal{G}(\mu,\sigma,c,d) & \text{otherwise} \end{cases}, \tag{5}$$

where $\mathcal{G}(\mu,\sigma,c,d)$ is an ordinary Gaussian truncated on $[c,d]$. We enforce this cutoff to prevent infeasibly narrow Gaussians and models that peak significantly outside the bounds, which lead to numerical difficulties and have ambiguous physical interpretations.

2.2 $\chi_{\rm eff}$ spin model

Because spin magnitudes are not measured precisely, we probe the same correlation using the effective dimensionless spin parameter $\chi_{\rm eff}$, the mass-weighted average of the spin component aligned with the orbital angular momentum, which is measured with much greater certainty. If we assume, as in our astrophysical models, that only the spun-up star has significant spin, then $\chi_{\rm eff}$ is a good proxy for a_A. This model, which we call `chieff`, models $\chi_{\rm eff}$ as a Gaussian on $[-1,1]$ that is again allowed to vary linearly with m_A:

$$\pi(\chi_{\rm eff}\,|\,\Lambda, m_A) = \mathcal{N}(\chi_{\rm eff};\,\mu(m_A,\Lambda), 10^{\log\sigma(m_A,\Lambda)}, -1, 1) \tag{6}$$

$$\mu(m_A,\Lambda) = \mu_0 + \delta_\mu\left(\frac{m_A}{10\,M_\odot} - 1\right) \tag{7}$$

$$\log\sigma(m_A,\Lambda) = \log\sigma_0 + \delta_{\log\sigma}\left(\frac{m_A}{10\,M_\odot} - 1\right). \tag{8}$$

We enforce a similar cutoff as in Equation 5, except we set $\mathcal{N}(\chi_{\rm eff}) = 0$ when $\mu \notin [-1,1]$. This model has 4 spin hyperparameters, $\Lambda = [\mu_0, \delta_\mu, \log\sigma_0, \delta_{\log\sigma}]$.

2.3 Alternate $\chi_{\rm eff}$ spin models

Finally, we explore two alternative models for $\chi_{\rm eff}$. The model is the same as the `chieff` model, but we instead allow $\chi_{\rm eff}$ to vary with the total mass $m_{\rm tot}$ (`chieff_totalmass`) and the primary mass m_1 (`chieff_m1`). The `chieff_m1` model is identical to one of the models explored in [8], and we include this model as a test of validation for our results.

The equations governing this model are identical to Equations 6-8, except the `chieff_totalmass` model has a pivot mass of $m_{\rm tot} = 20\,M_\odot$, such that

$$\mu(m_{\rm tot},\Lambda) = \mu_0 + \delta_\mu\left(\frac{m_{\rm tot}}{20\,M_\odot} - 1\right) \tag{9}$$

$$\log\sigma(m_{\rm tot},\Lambda) = \log\sigma_0 + \delta_{\log\sigma}\left(\frac{m_{\rm tot}}{20\,M_\odot} - 1\right). \tag{10}$$

3 Method

To perform the hierarchical inference, we use the Python hierarchical inference code `gwpopulation` [29], with the `dynesty` nested sampler [25] as implemented by `bilby` [4].

To create a simulated BBH catalog, we assume perfect detections, such that we have one posterior sample per event without error, and no selection effects. This assumption of perfect detections is reasonable to what we could expect from 3rd-generation (3G) detectors [20]. Therefore, we perform hierarchical inference with no selection effects and a flat PE prior. We draw $N = 1000$ events for each mock catalog. We opt to leave out fitting the redshift distribution for simplicity, as it is independent of other components of the model. To draw m_A and m_B, we first draw m_1 and m_2 from the `Power Law + Peak` mass model. Then, we randomly assign $m_1 = m_A$ (and $m_2 = m_B$) with a probability of $p = 20\%$, and correspondingly $m_1 = m_B$ (and $m_2 = m_A$) with a probability of $1 - p = 80\%$. This is motivated by the idea that it is the secondary star which is tidally spun-up.

We begin as a test of validation by drawing directly from the `a_A` and `chieff_mass1` models, then performing hierarchical inference with those corresponding models. We pick true values of the hyperparameters and draw $N = 1000$ events from the resulting model distribution to make our mock catalog.

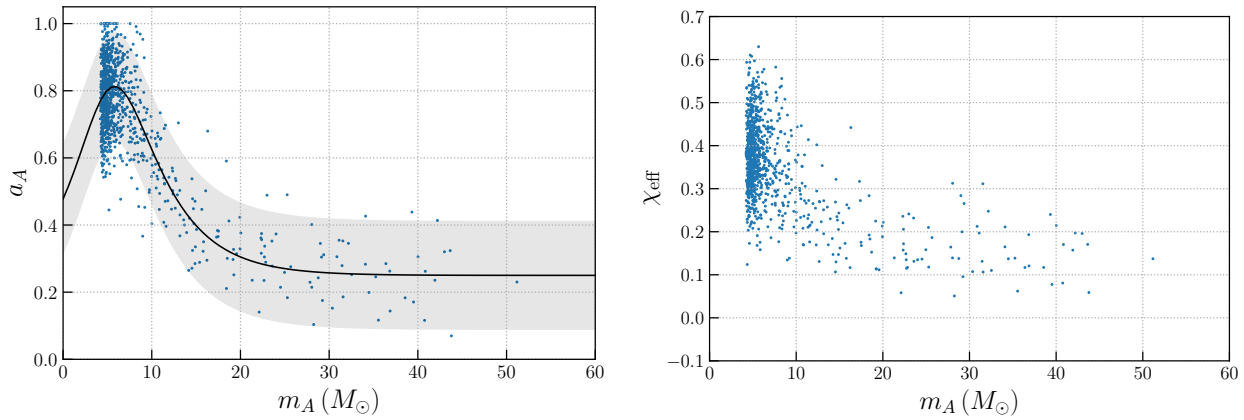

(a) (b)

Figure 1: A scatter plot of the mass-spin correlations in our mock BBH catalog. (a) plots the spin magnitude (a_A) as a function of the mass (m_A) of the higher spinning star; the black line shows the relationship parameterized by Equation 11, along with the 90% confidence intervals of the Gaussian noise (corresponding to $\pm 1.6\sigma = \pm 0.16$). (b) plots the effective spin parameter of the simulated BBH system ($\chi_{\rm eff}$) as a function of the mass of the higher spinning star (m_A).

Next, we create a mock catalog with mass-spin correlations drawn from a distribution motivated by Figure 8 of [6]. We parameterize this distribution with the relation

$$a_A(m_A) = \frac{A\exp(-Bm_A)}{1+\exp(-K(m_A - m_0))} + C. \tag{11}$$

We use values $A = 3$, $B = 0.2$, $K = 0.5$, $m_0 = 5$, and $C = 0.25$, which approximately matches a BBH progenitor system with sub-solar metallicity and an initial period of 0.3 days. We draw $N = 1000$ values of m_A and m_B with the method described above. We assign values of a_A by implementing 11 and adding Gaussian noise with standard deviation 0.1, in order to model the assumption that the universe does not have a one-to-one mapping of this correlation. We assign values of a_B by drawing from a Gaussian truncated on $[0, a_A]$ centered at 0 with a true value of $\sigma_B = 0.05$. To ensure that $a_A \in [0, 1]$, we set all points with $a_A > 1$ to $a_A = 1$, and all points with $a_A \leq 0$ to points drawn from a Gaussian truncated on $[0, 1]$ centered at 0 with standard deviation

0.05, such that stars which are not tidally spun up are drawn from a distribution identical to the a_B distribution, which represents the spin distribution of BHs born without tidal spin-up.

We fit both the `a_A` and `chieff` models to this mock catalog. To assign a value of $\chi_{\rm eff}$ to each mock observation, we must additionally model the spin tilt distribution, where the tilt angle θ for each BH is defined as the angle between the BH's angular momentum and the orbital angular momentum. We assign values of $\cos\theta_A$ and $\cos\theta_B$ by independently drawing from a Gaussian truncated on $[-1, 1]$ with mean 1 and standard deviation 0.2, to capture the expectation that the BH spins will be aligned with the orbital angular momentum in isolated evolutionary channels. We can then calculate $\chi_{\rm eff}$ with

$$\chi_{\rm eff} = \frac{m_A \cos\theta_A + m_B \cos\theta_B}{m_A + m_B}. \tag{12}$$

Figure 1 shows a scatter plot of this mock catalog, illustrating the mass spin correlations.

4 Injection Results

First, we are able to correctly recover the true values of the hyperparameters within the 90% symmetric credible interval when we perform hierarchical inference on mock BBHs drawn directly from the `a_A` and `chieff_m1` models with the corresponding models. Figure 2 shows the trace plots and 90% credible intervals of the posterior variation of the spin Gaussian mean and width with mass. No correlation is found in the absence of a true correlation, and a correlation (of the correct magnitude) is found in the presence of a true correlation, demonstrating the validity of our analysis. We still note, however, that caution must be used in any such hierarchical inference of a finite number of detections; biased realizations of the mock catalog from the small number statistics of the high mass tail of the BBH distribution can lead to incorrect recoveries of the hyperparameters of the true underlying distribution. Although not shown in Figure 2, we also correctly recover the true value of $\sigma_B = 0.2$, the width of the a_B distribution, which represents the distribution of spins of BHs which do not experience tidal spin-up.

Next, we hierarchically analyze with the `a_A` model the mock catalog illustrated in Figure 1, which is drawn from an astrophysically-motivated distribution. Here, the model is mis-specified: the model which we fit to the data is different from the true underlying model. The corner plot of the hyperparameters along with the 90% confidence intervals are given in Figure 3(c). The true value of $\sigma_B = 0.2$, which is reasonably close to the recovered value given the mis-specification of the a_A model. As shown in Figure 3(a), we recover with 90% confidence non-zero variation of the a_A Gaussian mean as a function of m_A. Therefore, under this model for the underlying astrophysical distribution with perfect detections, a linear correlation is sufficient to detect the mass-spin correlations encoded in tidal spin up. The linear correlation which we recover appears to be consistent with the true mean of the a_A distribution at a given m_A, given by the green dotted line. The hyperposterior also favors a spin distribution that broadens with m_A, as shown with the increasing Gaussian width with m_A in Figure 3(b). This is likely a consequence of the model mis-specification. The linear model is anchored on the pivot point of $m_A = 10\,M_\odot$, which was chosen to be near where most BBHs are located in parameter space. Because the true underlying distribution is non-linear, the true correlation deviates from the linear model as we move away from the pivot point, forcing the Gaussian to broaden to accommodate the mock detections at high m_A. This is then a generic feature of fitting a Gaussian whose width and mean is allowed to vary linearly to data with a non-linear correlation and fewer points away from the pivot point. This implies a caveat when viewing previous results which have found broadening distributions of BBH parameters with mass (e.g. [8]).

5 Inference on GWTC-3 data

We perform hierarchical inference on the 69 BBHs in the GWTC-3 catalog with False Alarm Rate (FAR) < 1 yr^{-1} [2] for each model. We use the `C01:IMRPhenomXPHM` datasets from the publicly-released individual event posterior samples published in the GWTC-2.1 [30] and GWTC-3 [31] data releases. We calculate the PE prior at the posterior sample points analytically, using the Jacobian developed by [9] to transform from a flat isotropic spin prior to a prior in $\chi_{\rm eff}$. To account for selection effects, we use the method described in [12] to compute the selection term $\alpha(\Lambda)$. We use the search sensitivity samples from the publicly-released simulated injection campaign [11], and consider a sample found using the same criteria as the GWTC-3 data release, i.e. if the optimal SNR $\rho_{\rm opt} > 10$ for O1 and O2, or if $\mathrm{FAR}_{\rm min} < 1$ yr^{-1} for O3, where $\mathrm{FAR}_{\rm min}$ is the minimum FAR

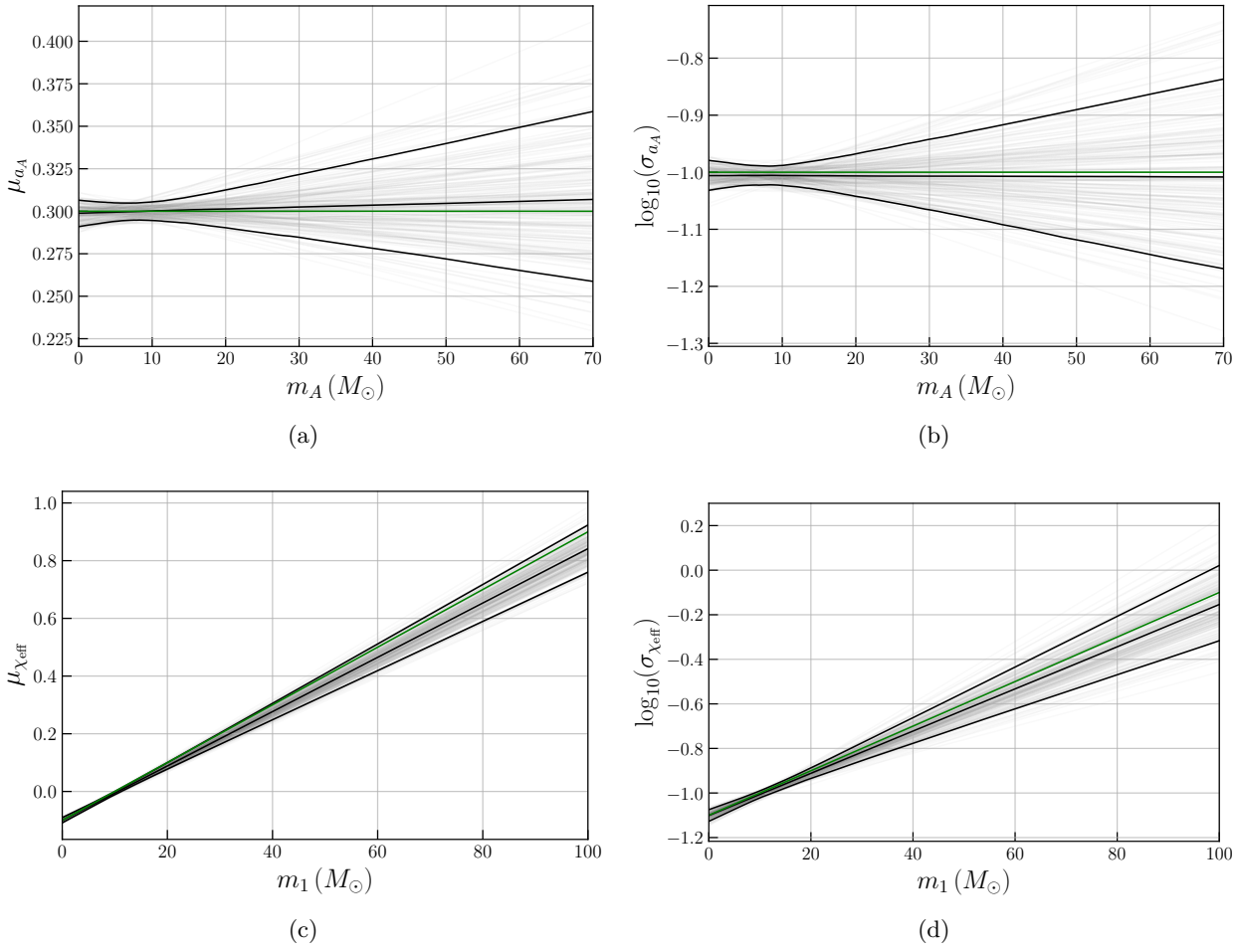

Figure 2: The results of the `a_A` (first row) and `chieff_totalmass` (second row) models on a mock catalog of $N = 1000$ events with no noise or selection effects, showing the mean (a, c) and log standard deviation (b, d) of the a_A and $\chi_{\rm eff}$ truncated Gaussians as a function of m_A and m_1, respectively. Solid black lines show the median and 90% symmetric credible intervals, faded gray lines show trace plots of 200 random samples from the hyperposterior, and the green line shows the true mass-spin correlation. For all analyses, the true variation of the mean and standard deviation with mass is recovered within the 90% credible interval.

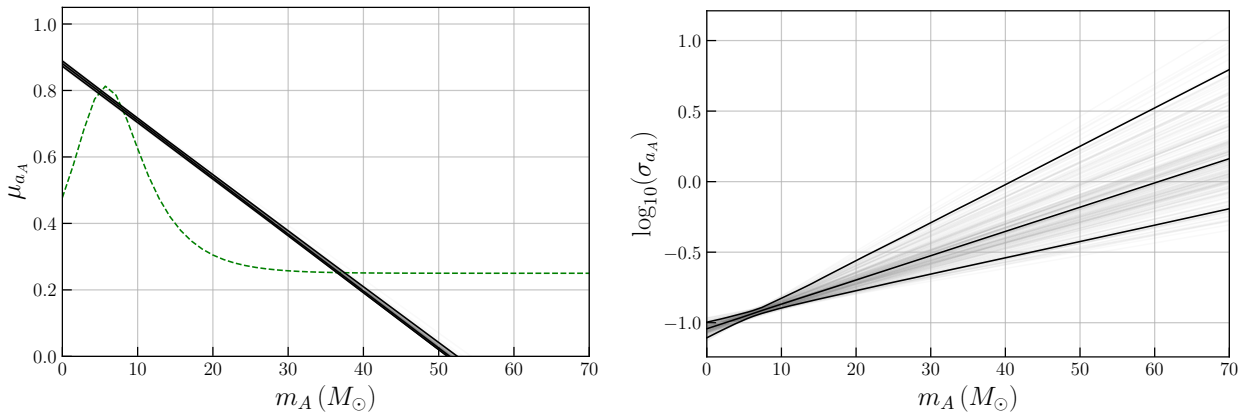

(a) (b)

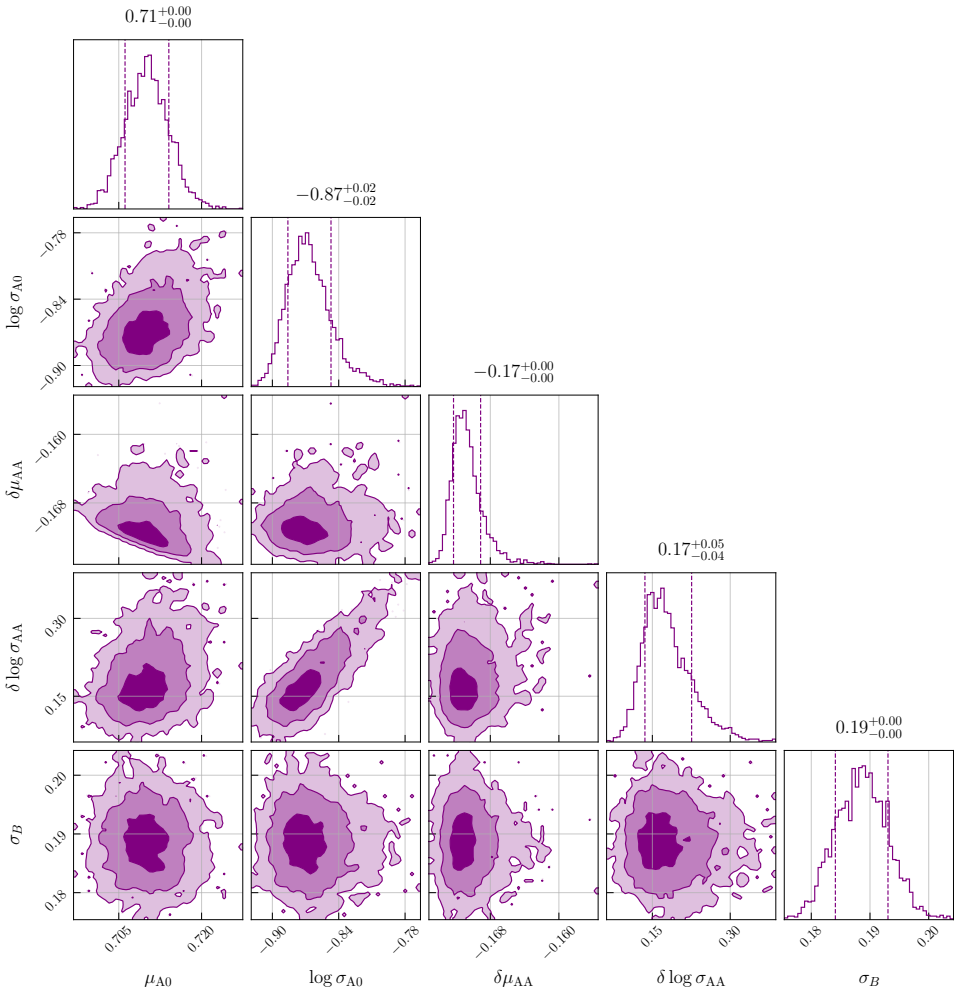

(c)

Figure 3: The results of the `a_A` model on the mock catalog in Figure 1 showing the mean (a) and log standard deviation (b) of the a_A truncated Gaussian as a function of m_A. As in Figure 2, the solid black lines show the median and 90% credible intervals. The green dotted line in (a) show the true mean of the underlying distribution given by Equation 11. In (c), we show the corner plot of the hyperparameters.

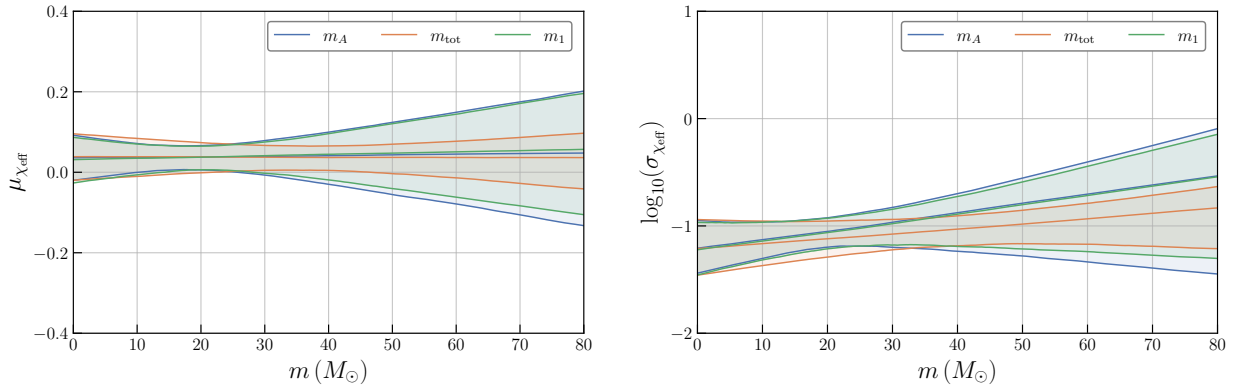

(a) (b)

Figure 4: The mean (a) and log standard deviation (b) of the $\chi_{\rm eff}$ truncated Gaussian for all three models, `chieff`, `chieff_totalmass`, and `chieff_mass1`, on GWTC-3 data as a function of m_A, $m_{\rm tot}$, and m_1, respectively. Solid lines show the median and 90% symmetric credible intervals. We find no evidence of any variation of $\chi_{\rm eff}$ with m_A, $m_{\rm tot}$, or m_1.

across all search pipelines.

We have found that there can be significant regions of parameter space that have a very low number of effective Monte-Carlo samples ($N_{\rm eff}$), especially at negative values of $\delta \log \sigma$, whose narrow Gaussians are poorly sampled from the individual event $\chi_{\rm eff}$ posteriors. To remedy this issue, we assign a likelihood of 0 to regions of parameter space with $N_{\rm eff} < N$, where N is the number of events, and switch from using `C01:Mixed` to `C01:IMRPhenomXPHM` PE samples for our analysis of GWTC-3 data in order to have more samples. We implement this with the `MinimumEffectiveSamplesLikelihood` class from `gwpopulation_pipe` [26], the interface package to `gwpopulation`. This effect is important in the hierarchical inference with the `a_A` model. For reasonable values of $\mu_{a_A} \approx 0.1 - 0.4$, $N_{\rm eff} \sim \mathcal{O}(1)$ for all non-positive values. Because the likelihood is set to 0 in that region of parameter space, the posterior a_A distribution is forced to broaden with m_A. Therefore, it is currently not possible to reliably probe the `a_A` model parameter space with the given set of GWTC-3 PE samples.

Figure 4 shows the posterior mean and log standard deviation of the $\chi_{\rm eff}$ truncated Gaussian as a function of m_A, $m_{\rm tot}$, and m_1, from inference with the `chieff`, `chieff_totalmass`, `chieff_mass1` models, respectively. Consistent with the results of [8], we find no evidence of $\chi_{\rm eff}$ varying as a function of mass for any of our models. The $\chi_{\rm eff}$ distribution likely peaks at a small, positive number, also consistent with the results of [2].

6 Conclusion and Next Steps

In this project, we construct several models that target the mass-spin correlation expected from the tidal spin-up of BBH progenitor systems. While models that look for a correlation between $\chi_{\rm eff}$ and mass are present in the current literature, we present a novel use of the spin-sorting method pioneered by [7] to look for correlations between the spin magnitude (a_A) and mass (m_A) of the tidally spun-up star. These models only look for a first-order linear correlation, as has been done previously in the literature when looking for correlations between BBH parameters, and are therefore agnostic to the true shape of the correlation. We demonstrate the validity of performing

hierarchical inference with these models with a simplified injection study. We then investigate the recovery of a correlation with a non-linear shape, motivated by the modelling results of [21]. We find that a non-correlation is excluded with 90% confidence, and that the correlation we do recover is consistent with the injected distribution. Furthermore, we find that the broadening of the spin distribution Gaussian with mass can be a feature of model mis-specification, rather than a result of true broadening. We also perform hierarchical inference on GWTC-3 data with these models. We are unable to probe the full parameter space of the `a_A` model due to an insufficient number of effective PE samples, and we find no evidence of a correlation of $\chi_{\rm eff}$ with mass.

The immediate next step of this project is to better model the mass-spin correlation in tidally spun-up BBH merger systems. In this work, we picked a distribution that roughly matched the result from a single value of the initial orbital period $P_{\mathrm{orb},i}$, rather than including a range of initial periods. To add the dimension of initial period into our model, we have created the following analytic approximation for the BH spin that results from tidal spin-up, $a_{\rm TSU}$:

$$a_{\rm TSU}(m_A, P_{\mathrm{orb},i}) = \begin{cases} a_{\text{no TSU}} + A(P_{\mathrm{orb},i}) \left[\frac{\exp(-0.2\, m_A/M_\odot)}{1+\exp(-0.5(m_A/M_\odot - 6))}\right] + C(P_{\mathrm{orb},i}) & \text{if } P_{\mathrm{orb},i} < 1 \text{ day} \\ a_{\text{no TSU}} & \text{if } P_{\mathrm{orb},i} \geq 1 \text{ day} \end{cases} \tag{13}$$

$$\text{where } A(P) = 6(1 - P/\text{day}))^2, \quad C(P) = 0.7(1 - P/\text{day}))^3. \tag{14}$$

Here, $a_{\text{no TSU}}$ represents the natal BH spin in the absence of tidal spin-up. The lack of tidal spin-up from systems with higher orbital periods and therefore larger orbital separations is also supported by [6]. To model $a_{\text{no TSU}}$, we use the model for a_B, just without the enforcement that $a_A > a_B$, since both represent the natal BH spin in the absence of tidal spin-up:

$$p(a_{\text{no TSU}}|\sigma_B) = \mathcal{N}_{1/2}(a_{\text{no TSU}};\, 0, \sigma_B, 0, 1) \tag{15}$$

where $\mathcal{N}_{1/2}(a;\, \mu, \sigma, c, d)$ is a half-Gaussian with mean μ and standard deviation σ truncated on $[c, d]$. Therefore, we can model the correlation of a_A with m_A with the following probability distribution:

$$p(a_A|m_A,\, P_{\mathrm{orb},i},\, \sigma_B) = \mathcal{N}_{1/2}(a_A;\, a_{\rm TSU}(m_A, P_{\mathrm{orb},i}), \sigma_B, 0, 1) \tag{16}$$

It is then imperative to try to model the distribution of initial periods, $p(P_{\mathrm{orb},i})$. Currently, the idea is to model the distribution of zero-age main sequence (ZAMS) separations as a log-uniform distribution [22], which can be converted to a distribution in $P_{\mathrm{orb},i}$ with Kepler's 3rd law, given the BBH massses. We can assume that little angular momentum is lost during the binary evolution until the system becomes a BBH system, such that the ZAMS initial period is the same as the initial period of the BBH progenitor system, which is what was used in [21]. We can choose a cutoff for the minimum $P_{\mathrm{orb},i}$ in $p(P_{\mathrm{orb},i})$ of 0.3 days. The maximum $P_{\mathrm{orb},i}$, $P_{\rm max}$, is imposed by a limit on the merger time. If the initial separation is too wide, it cannot have merged between the redshift that that it formed and the redshift at which we observe it in the first place. For a given initial period, we can approximate the merger delay time $t_{\rm merge}$ by using the quadrupole radiation formula and assuming circular Keplerian orbits; the result is a power law dependence on the BH masses and $t_{\rm merge}$. Therefore, we can calculate $P_{\rm max}$ by calculating the maximum delay time allowed by the merger's redshift (where the allowed delay time is limited by the Hubble time), weighting with a model for the star formation rate, and calculating the initial period corresponding to $t_{\rm merge}$ equal to that maximum delay time given the BH masses. Even in accounting for these astrophysical selection effects, there are many assumptions going to this calculation, and the resulting correlation

would still be subject to significant modelling uncertainties. Nonetheless, it would be interesting to see the resulting mass-spin correlation of merging field BBHs from tidal spin-up.

The other immediate next step would be to make the mock BBH catalog more realistic. The goal of this project is ultimately to make predictions for future detectors, from future observing runs to 3G detectors. To do so, we will have to take into account the detection efficiencies and detector noise of these future detectors.

The final, and arguably most interesting, extension of this project would be to investigate the biases of this hierarchical inference that result from contamination from other sub-populations. A sub-population of dynamical mergers, for example, could introduce a significant number of detections with no mass-spin correlation, with a subset of hierarchical mergers with a mass-spin correlation. We can model the astrophysical distribution with a mixing fraction of BBHs which do not experience tidal spin-up and a mixing fraction of hierarchical mergers.

7 Acknowledgements

This work was supported by the National Science Foundation Research Experience for Undergraduates (NSF REU) program, the LIGO Laboratory Summer Undergraduate Research Fellowship program (NSF LIGO), and the California Institute of Technology Student-Faculty Programs. Additionally, I would like to thank my advisors Jacob Golomb and Alan Weinstein for their invaluable support and advice throughout my summer project.

References

[1] B. P. Abbott et al. "Observation of Gravitational Waves from a Binary Black Hole Merger". In: Phys. Rev. Lett. 116.6, 061102 (Feb. 2016), p. 061102. DOI: 10.1103/PhysRevLett.116.061102. arXiv: 1602.03837 [gr-qc].

[2] R. Abbott et al. "Population of Merging Compact Binaries Inferred Using Gravitational Waves through GWTC-3". In: *Physical Review X* 13.1, 011048 (Jan. 2023), p. 011048. DOI: 10.1103/PhysRevX.13.011048. arXiv: 2111.03634 [astro-ph.HE].

[3] F. Acernese et al. "Advanced Virgo: a second-generation interferometric gravitational wave detector". In: *Classical and Quantum Gravity* 32.2, 024001 (Jan. 2015), p. 024001. DOI: 10.1088/0264-9381/32/2/024001. arXiv: 1408.3978 [gr-qc].

[4] Gregory Ashton et al. "BILBY: A User-friendly Bayesian Inference Library for Gravitational-wave Astronomy". In: ApJS 241.2, 27 (Apr. 2019), p. 27. DOI: 10.3847/1538-4365/ab06fc. arXiv: 1811.02042 [astro-ph.IM].

[5] Vishal Baibhav, Zoheyr Doctor, and Vicky Kalogera. "Dropping Anchor: Understanding the Populations of Binary Black Holes with Random and Aligned-spin Orientations". In: ApJ 946.1, 50 (Mar. 2023), p. 50. DOI: 10.3847/1538-4357/acbf4c. arXiv: 2212.12113 [astro-ph.HE].

[6] Simone S. Bavera, Michael Zevin, and Tassos Fragos. "Approximations of the Spin of Close Black Hole-Wolf-Rayet Binaries". In: *Research Notes of the American Astronomical Society* 5.5, 127 (May 2021), p. 127. DOI: 10.3847/2515-5172/ac053c. arXiv: 2105.09077 [astro-ph.HE].

[7] Sylvia Biscoveanu et al. "New Spin on LIGO-Virgo Binary Black Holes". In: Phys. Rev. Lett. 126.17, 171103 (Apr. 2021), p. 171103. DOI: 10.1103/PhysRevLett.126.171103. arXiv: 2007.09156 [astro-ph.HE].

[8] Sylvia Biscoveanu et al. "The Binary Black Hole Spin Distribution Likely Broadens with Redshift". In: ApJ 932.2, L19 (June 2022), p. L19. DOI: 10.3847/2041-8213/ac71a8. arXiv: 2204.01578 [astro-ph.HE].

[9] T. A. Callister. "A Thesaurus for Common Priors in Gravitational-Wave Astronomy". In: *arXiv e-prints*, arXiv:2104.09508 (Apr. 2021), arXiv:2104.09508. DOI: 10.48550/arXiv.2104.09508. arXiv: 2104.09508 [gr-qc].

[10] Thomas A. Callister et al. "Who Ordered That? Unequal-mass Binary Black Hole Mergers Have Larger Effective Spins". In: ApJ 922.1, L5 (Nov. 2021), p. L5. DOI: 10.3847/2041-8213/ac2ccc. arXiv: 2106.00521 [astro-ph.HE].

[11] LIGO Scientific Collaboration, Virgo Collaboration, and KAGRA Collaboration. *GWTC-3: Compact Binary Coalescences Observed by LIGO and Virgo During the Second Part of the Third Observing Run — O1+O2+O3 Search Sensitivity Estimates*. LIGO Laboratory and Advanced LIGO are funded by the United States National Science Foundation (NSF) as well as the Science and Technology Facilities Council (STFC) of the United Kingdom, the Max-Planck-Society (MPS), and the State of Niedersachsen/Germany for support of the construction of Advanced LIGO and construction and operation of the GEO600 detector. Additional support for Advanced LIGO was provided by the Australian Research Council. Virgo is funded, through the European Gravitational Observatory (EGO), by the French Centre National de Recherche Scientifique (CNRS), the Italian Istituto Nazionale di Fisica Nucleare (INFN) and the Dutch Nikhef, with contributions by institutions from Belgium, Germany, Greece, Hungary, Ireland, Japan, Monaco, Poland, Portugal, Spain. The construction and operation of KAGRA are funded by Ministry of Education, Culture, Sports, Science and Technology (MEXT), and Japan Society for the Promotion of Science (JSPS), National Research Foundation (NRF) and Ministry of Science and ICT (MSIT) in Korea, Academia Sinica (AS) and the Ministry of Science and Technology (MoST) in Taiwan. Zenodo, May 2023. DOI: 10.5281/zenodo.7890398. URL: https://doi.org/10.5281/zenodo.7890398.

[12] Will M. Farr. "Accuracy Requirements for Empirically Measured Selection Functions". In: *Research Notes of the American Astronomical Society* 3.5, 66 (May 2019), p. 66. DOI: 10.3847/2515-5172/ab1d5f. arXiv: 1904.10879 [astro-ph.IM].

[13] Maya Fishbach, Daniel E. Holz, and Will M. Farr. "Does the Black Hole Merger Rate Evolve with Redshift?" In: ApJ 863.2, L41 (Aug. 2018), p. L41. DOI: 10.3847/2041-8213/aad800. arXiv: 1805.10270 [astro-ph.HE].

[14] Maya Fishbach, Chase Kimball, and Vicky Kalogera. "Limits on Hierarchical Black Hole Mergers from the Most Negative χ_{eff} Systems". In: ApJ 935.2, L26 (Aug. 2022), p. L26. DOI: 10.3847/2041-8213/ac86c4. arXiv: 2207.02924 [astro-ph.HE].

[15] Gabriele Franciolini and Paolo Pani. "Searching for mass-spin correlations in the population of gravitational-wave events: The GWTC-3 case study". In: Phys. Rev. D 105.12, 123024 (June 2022), p. 123024. DOI: 10.1103/PhysRevD.105.123024. arXiv: 2201.13098 [astro-ph.HE].

[16] Gabriele Franciolini et al. "Searching for a subpopulation of primordial black holes in LIGO-Virgo gravitational-wave data". In: Phys. Rev. D 105.8, 083526 (Apr. 2022), p. 083526. DOI: 10.1103/PhysRevD.105.083526. arXiv: 2105.03349 [gr-qc].

[17] Jim Fuller and Linhao Ma. "Most Black Holes Are Born Very Slowly Rotating". In: ApJ 881.1, L1 (Aug. 2019), p. L1. DOI: 10.3847/2041-8213/ab339b. arXiv: 1907.03714 [astro-ph.SR].

[18] Davide Gerosa and Maya Fishbach. "Hierarchical mergers of stellar-mass black holes and their gravitational-wave signatures". In: *Nature Astronomy* 5 (July 2021), pp. 749–760. DOI: 10.1038/s41550-021-01398-w. arXiv: 2105.03439 [astro-ph.HE].

[19] Jaxen Godfrey, Bruce Edelman, and Ben Farr. "Cosmic Cousins: Identification of a Subpopulation of Binary Black Holes Consistent with Isolated Binary Evolution". In: *arXiv e-prints*, arXiv:2304.01288 (Apr. 2023), arXiv:2304.01288. DOI: 10.48550/arXiv.2304.01288. arXiv: 2304.01288 [astro-ph.HE].

[20] Francesco Iacovelli et al. "Forecasting the Detection Capabilities of Third-generation Gravitational-wave Detectors Using GWFAST". In: ApJ 941.2, 208 (Dec. 2022), p. 208. DOI: 10.3847/1538-4357/ac9cd4. arXiv: 2207.02771 [gr-qc].

[21] Linhao Ma and Jim Fuller. "Tidal Spin-up of Black Hole Progenitor Stars". In: ApJ 952.1, 53 (July 2023), p. 53. DOI: 10.3847/1538-4357/acdb74. arXiv: 2305.08356 [astro-ph.HE].

[22] Ilya Mandel and Alison Farmer. "Merging stellar-mass binary black holes". In: Phys. Rep. 955 (Apr. 2022), pp. 1–24. DOI: 10.1016/j.physrep.2022.01.003. arXiv: 1806.05820 [astro-ph.HE].

[23] Ethan Payne et al. "Searching for anisotropy in the distribution of binary black hole mergers". In: Phys. Rev. D 102.10, 102004 (Nov. 2020), p. 102004. DOI: 10.1103/PhysRevD.102.102004. arXiv: 2006.11957 [astro-ph.CO].

[24] April Qiu Cheng, Michael Zevin, and Salvatore Vitale. "What You Don't Know Can Hurt You: Use and Abuse of Astrophysical Models in Gravitational-wave Population Analyses". In: *arXiv e-prints*, arXiv:2307.03129 (July 2023), arXiv:2307.03129. DOI: 10.48550/arXiv.2307.03129. arXiv: 2307.03129 [astro-ph.HE].

[25] Joshua S. Speagle. "DYNESTY: a dynamic nested sampling package for estimating Bayesian posteriors and evidences". In: MNRAS 493.3 (Apr. 2020), pp. 3132–3158. DOI: 10.1093/mnras/staa278. arXiv: 1904.02180 [astro-ph.IM].

[26] Colm Talbot. "GWPopulation pipe". In: (Nov. 2021). DOI: 10.5281/zenodo.5654673. URL: https://git.ligo.org/RatesAndPopulations/gwpopulation_pipe.

[27] Colm Talbot and Eric Thrane. "Determining the population properties of spinning black holes". In: Phys. Rev. D 96.2, 023012 (July 2017), p. 023012. DOI: 10.1103/PhysRevD.96.023012. arXiv: 1704.08370 [astro-ph.HE].

[28] Colm Talbot and Eric Thrane. "Measuring the Binary Black Hole Mass Spectrum with an Astrophysically Motivated Parameterization". In: ApJ 856.2, 173 (Apr. 2018), p. 173. DOI: 10.3847/1538-4357/aab34c. arXiv: 1801.02699 [astro-ph.HE].

[29] Colm Talbot et al. "Parallelized inference for gravitational-wave astronomy". In: Phys. Rev. D 100.4, 043030 (Aug. 2019), p. 043030. DOI: 10.1103/PhysRevD.100.043030. arXiv: 1904.02863 [astro-ph.IM].

[30] The LIGO Scientific Collaboration et al. "GWTC-2.1: Deep Extended Catalog of Compact Binary Coalescences Observed by LIGO and Virgo During the First Half of the Third Observing Run". In: *arXiv e-prints*, arXiv:2108.01045 (Aug. 2021), arXiv:2108.01045. DOI: 10.48550/arXiv.2108.01045. arXiv: 2108.01045 [gr-qc].

[31] The LIGO Scientific Collaboration et al. "GWTC-3: Compact Binary Coalescences Observed by LIGO and Virgo During the Second Part of the Third Observing Run". In: *arXiv e-prints*, arXiv:2111.03606 (Nov. 2021), arXiv:2111.03606. DOI: 10.48550/arXiv.2111.03606. arXiv: 2111.03606 [gr-qc].

[32] Eric Thrane and Colm Talbot. "An introduction to Bayesian inference in gravitational-wave astronomy: Parameter estimation, model selection, and hierarchical models". In: PASA 36, e010 (Mar. 2019), e010. DOI: 10.1017/pasa.2019.2. arXiv: 1809.02293 [astro-ph.IM].

[33] L. A. C. van Son et al. "No Peaks without Valleys: The Stable Mass Transfer Channel for Gravitational-wave Sources in Light of the Neutron Star-Black Hole Mass Gap". In: ApJ 940.2, 184 (Dec. 2022), p. 184. DOI: 10.3847/1538-4357/ac9b0a. arXiv: 2209.13609 [astro-ph.HE].

[34] Salvatore Vitale, Sylvia Biscoveanu, and Colm Talbot. "Spin it as you like: The (lack of a) measurement of the spin tilt distribution with LIGO-Virgo-KAGRA binary black holes". In: A&A 668, L2 (Dec. 2022), p. L2. DOI: 10.1051/0004-6361/202245084. arXiv: 2209.06978 [astro-ph.HE].

[35] Michael Zevin and Simone S. Bavera. "Suspicious Siblings: The Distribution of Mass and Spin across Component Black Holes in Isolated Binary Evolution". In: ApJ 933.1, 86 (July 2022), p. 86. DOI: 10.3847/1538-4357/ac6f5d. arXiv: 2203.02515 [astro-ph.HE].

[36] Michael Zevin et al. "One Channel to Rule Them All? Constraining the Origins of Binary Black Holes Using Multiple Formation Pathways". In: ApJ 910.2, 152 (Apr. 2021), p. 152. DOI: 10.3847/1538-4357/abe40e. arXiv: 2011.10057 [astro-ph.HE].